



Comparative sustainability analysis of serpentine flow-field and straight channel PEM fuel cell designs

Mohamed-Amine Babay¹ · Mustapha Adar¹ · Ahmed Chebak² · Mustapha Mabrouki¹

Received: 26 October 2023 / Revised: 27 April 2024 / Accepted: 13 June 2024 / Published online: 2 July 2024

© The Author(s) under exclusive licence to The Society for Reliability Engineering, Quality and Operations Management (SREQOM), India and The Division of Operation and Maintenance, Lulea University of Technology, Sweden 2024

Abstract This study employed numerical analysis to evaluate the sustainability of Serpentine Flow-Field and Straight channel PEM fuel cells, focusing on critical parameters such as reactant velocity, temperature, current density, water content, membrane hydration, and polarization behavior curve. The model incorporated the transportation of gases, water, and electrical current within the fuel cell's layers, emphasizing the importance of optimizing performance and reducing costs through the design of the membrane electrode assembly (MEA). Utilizing the finite element method and ANSYS Fluent, the model allowed for adjustments in parameters such as membrane thickness and protonic conductivity coefficient, both of which significantly impact cell performance. The findings indicated that both fuel cell designs performed well, with a slight advantage observed for the Straight channel configuration in terms of production. However, the performance difference was relatively small, with the Straight channel design outperforming the Serpentine Flow-Field configuration by approximately 5% in terms of production. Despite this slight discrepancy, both designs demonstrated good performance overall. Moreover, the study underscored the critical role of MEA design optimization in achieving maximum performance and cost-effectiveness. While Straight channel PEM fuel cells may be slightly more cost-effective for certain applications, Serpentine Flow-Field PEM fuel cells offer enhanced efficiency and durability, making them preferable in many scenarios. In

conclusion, this research provides valuable insights into the sustainability of these two fuel cell designs, indicating that while both are viable options, Serpentine Flow-Field PEM fuel cells offer slightly better performance and durability, thus warranting consideration for future applications.

Keywords Hydrogen production · PEM fuel cells · Serpentine flow field · Straight channel · Modelling · CFD · ANSYS fluent

1 Introduction

Compared to other types of fuel cells, PEM fuel cells produce more power for a given volume and weight. This type of fuel cell requires little time to start due to low temperature, and this feature makes them the best option for in-vehicle applications as an alternative to diesel and gasoline internal combustion engines. These systems are also suitable for use in home generators, small power plants, transportation and military industries (Mei et al. 2022). Fuel cell applications range from low-power to high-power systems. Fuel cells are powered by hydrogen and therefore must be equipped with a hydrogen production system (Kyriakopoulos and Sebos 2023; Kyriakopoulos and Aravossis 2023). Increasing performance and improving water and thermal management are some of the challenging problems in the PEM fuel cells (Henriques et al. 2010). Numerical analyses in the fuel cell can include a complete study of the fuel cell system (Ahsan et al. 2021), the study of bipolar plates (Barnoon et al. 2022), the study of the gas diffusion layer (Kanchan et al. 2020), the study of the catalyst layer (Zhang et al. 2021) and the oxygen production system (Jia et al. 2021). Sun et al. (Sun et al. 2006) investigated a 3-D, steady, and single-phase flow of a PEM fuel cell with

✉ Mohamed-Amine Babay
mdamine.babay@gmail.com

¹ Laboratory of Industrial and Surface Engineering, Faculty of Science and Technologies, Sultan Moulay Slimane University, Beni Mellal, Morocco

² Green Tech Institute (GTI), Mohammed VI Polytechnic University, Benguerir, Morocco

a helical configuration. They studied pressure distribution and flow through the GDL. The gas flow channel with a trapezoidal cross-section was introduced in their study. The results showed that the aspect ratio of the trapezoidal cross-section has a significant effect on the flow rate. As this ratio increases, the throughput flow through the GDL increases. This ratio also has a large effect on the change in field pressure. Ahmed and Song (Ahmed and Sung 2008) simulated a PEM fuel cell with a three-dimensional, non-isothermal and raised membrane electrode assembly. In their study, the adjacent shoulders had different heights. The effect of variation of membrane electrode assembly on cell performance was investigated by maintaining the same reaction area and boundary conditions at high current densities. They found that the cathode voltage drop decreases significantly with increasing swelling of the membrane electrode set so that the reactants are more evenly distributed on the reaction surface.

X. D. Wang et al. (Wang et al. 2012) numerically investigated the effect of cathode channel shape on transmission features and performance of a PEM fuel cell in a 3-D model and two-phase flow. They found that at high operating voltages, cells with various channel configurations performed similarly. Atyabi and Afshari (Bernardi 1990) introduced a numerical model that provided a complete understanding of the basic principles of transfer phenomena in the fuel cell of a polymer membrane with a honeycomb flow field. The results showed that increasing the operating pressure leads to more oxygen distribution in the cathode electrode and increasing the permeability of the gas diffusion layer increases the uniformity of oxygen distribution and consequently the current density. Ghanbarian and Kermani (Mohammad Jafar Kermani 2014) studied a proton exchange membrane fuel cell considering the single-phase flow of the reactant-product mixture at the air cell side electrode. The results show that channel indentation can increase the oxygen concentration content at the surface of the catalyst layer by up to 18%. In 2015, Vazifeshenas et al. (Vazifeshenas et al. 2015) numerically investigated the effects of the flow field on improving the performance of a PEM fuel cell. They showed that changing the flow field design could still be used as a practical way to improve performance.

Hu et al. (Hu et al. 2004) designed a three-dimensional model that considers both liquid and dissolved water transport in a PEM fuel cell. Prior simulations were limited to low-humidity feed streams and constant temperature (Nguyen et al. 2004; Sivertsen and Djilali 2005). Wang et al. (Wang et al. 2003) and Djilali (Berning 2002) use a single-phase model but did not consider the effect of liquid water on gas diffusion electrode transport. The impact of liquid water remains unstudied. Verbrugge (Bernardi and Verbrugge 1992) and Springer et al. (Bernardi 1990) developed the initial 1D models for PEM fuel cells, which focused exclusively on changes across the membrane. These models were fundamental in developing

future multidimensional models and understanding fuel cell mechanisms. Fuller and Newman (Fuller and Newman 1993), Nguyen and White (Nguyen and White 1993), and Yi (Yi and Nguyen 1998) later created 2D models that included both membrane changes and bulk flow direction, emphasizing the importance of water and thermal management in achieving high fuel cell performance. While Gurau et al. (Gurau et al. 1998) used CFD to construct 2D models, they neglected the effect of ribs in flow channels. You et al. (You and Liu 2002) developed a 2D model that studied transport in regions with two-phase flow, but only considered the cathode side of a PEM fuel cell and included just the gas channel, diffuser, and catalyst layer. This model did not address two-phase transport on the anode side, water distribution in the membrane for humidification, or flooding in the gas diffuser near the rib area.

Monsef et al. (Tamerabet et al. 2017) investigated the effects of channel width, the number of coil channels, and flow direction on the consumption of reactants in a PEM fuel cell with cochlear flow field design numerically using FVM in cylindrical coordinates. Their findings show that the ratio of channel width to rib influences cell performance. The larger the ratio, the more important the contact area between the channel and the GDL, the more reactants penetrate the GDL, and the more uniform the distribution of reactants. Sun et al. (Sun et al. 2006) studied channel-to-channel flow in a PEM-fuel cell using a serpentine channel with a trapezoidal cross-sectional shape. Their results show that for both modes the pressure drop is significant but for cross-flow, the pressure drop tends to decrease across the channel. A literature review shows that robust studies have been performed in relation to fuel cell simulations. However, most studies focus on the study of physical parameters (relative humidity, cell voltage, stoichiometric ratio, mass flow rate, etc.) and their impact on fuel cell performance. This study develops a 3D numerical and isothermal model to analyze the impact of operating voltage on key factors within the core of a of a Serpentine Flow-Field, the straight channel Proton Exchange Membrane Fuel Cell (PEMFC). The model includes the transport of gases in the GDL, electric current, and water in the membrane. The study's key findings include the creation of a mathematical model for mass transfer in the PEMFC core, as well as the numerical solution of governing equations using ANSYS Fluent and MATLAB 2022a.

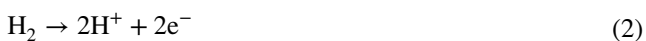
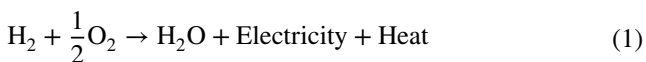
2 Mathematical description

2.1 Model description

PEM fuel cells utilize an electrochemical reaction between hydrogen and oxygen to produce electricity, heat, and water. Key to their function is the membrane electrode assembly (MEA), consisting of a proton exchange membrane (PEM),

anode, cathode, and catalyst layer. Hydrogen undergoes oxidation at the anode, producing protons and electrons. Protons pass through the PEM to the cathode, while electrons travel through an external circuit. At the cathode, oxygen combines with protons and electrons to form water. The generated electrical current powers devices or can be stored. Water vapor is the only byproduct. Efficiency depends on factors like PEM quality, electrode design, and reactant distribution (Babay et al. 2021). This section presents the model and equations employed to examine gas, water, and electrical current transport within various layers of the fuel cell. The equations encompass mass, momentum, and energy conservation, alongside the Nernst and Butler-Volmer equations.

The fuel cell operates by utilizing hydrogen as fuel and oxygen from the air as an oxidant, leading to a controlled reaction akin to the reverse of water electrolysis. This process generates electrical energy through the combustion of hydrogen (Babay et al. 2024b, 2024c).



A thorough investigation into water dynamics within fuel cell layers is essential for optimizing the efficiency and durability of PEM fuel cells under various operating conditions. The present model meticulously examines the steady-state transport of reactants and water within the fuel cell, providing a comprehensive analysis that covers both anode and cathode mass, as well as momentum transport phenomena, including for serpentine low-temperature PEM fuel cells (Fig. 1).

This investigation delves into the intricate network of flow channels, gas diffusion layers (GDLs), and gas diffusion

electrodes (GDEs), revealing the complex interactions governing the cell’s behavior. Additionally, the model expands its scope to include the nuanced realm of electrochemical currents, meticulously studying their impact within the GDLs, GDEs, and polymer membrane. By exploring these multifaceted aspects, the model aims to clarify the intricacies of transport processes and electrochemical phenomena, offering valuable insights into the performance and behavior of the fuel cell under examination. The analysis encompasses the entire spectrum of mass and momentum transport, providing a holistic perspective that contributes to a refined understanding of the cell’s operational dynamics, with specific parameters detailed in Tables 1 and 2.

2.2 Assumptions

The assumptions made for the equations are outlined as follows:

- Steady fluid flow within the fuel cell channel is assumed, a common practice in PEMFCs due to the absence of phase change modeling.
- The flow is presumed to be incompressible and laminar, justified by low pressure and velocity gradients.
- Gases are assumed to adhere to the ideal gas law, exhibiting behavior akin to ideal particles under various temperature and pressure conditions.
- Both cathode and anode are assumed to have 100% relative humidity, as higher fuel cell performance is associated with fully humid intake gases.
- Gravity’s influence is neglected, as convective and viscosity forces outweigh weight forces significantly.
- The porous media within the cell are treated as homogeneous and isotropic, a realistic assumption reflecting uniformity in material structure across all directions.

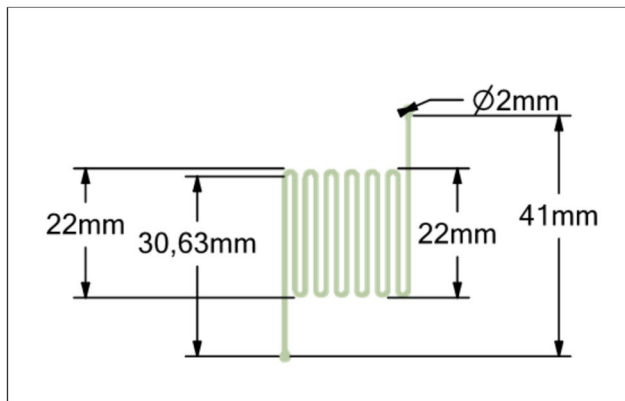


Fig. 1 Geometries of a Serpentine Flow-Field PEM-FC

Table 1 Operation parameters of the straight channel fuel cell section

Parameters	Units	Symbol	Case
Cell length	mm	L	10
Channel width/height	mm	W/H	0,5
Gas diffusion layer thickness	mm	DGDL	0,015
Catalyst layer thickness	mm	DCL	0,008
Membrane thickness	mm	DMEM	0,02

Table 2 Inlet mass fraction

Species	Value
Inlet H ₂ mass fraction	0.96
Inlet H ₂ O mass fraction	0.037
Inlet O ₂ mass fraction	0.202

- Darcy’s law is employed to model the porous medium, offering good accuracy in combination with laminar flow.
- The flow is simplified as single-phase, reducing simulation complexity and facilitating a clearer understanding of the problem’s physics.

2.3 Governing equations

The general form of the continuity equation is represented as follows (Babay et al. 2021, 2024a, 2023),

$$\begin{cases} \epsilon \nabla \cdot (\rho \vec{u}) = S_m \\ S_m = 0 \end{cases} \Rightarrow \nabla \cdot (\rho \vec{u}) = 0 \tag{4}$$

In Eq. (4), S_m represents the mass source, ρ represents the density, ϵ represents the porosity in the gas diffusion layer and the catalyst layer, and u represents the velocity. The fluid flow in the gas diffusion layer and the catalyst layer is in a porous medium, and there is a mass source in it because the chemical reaction of the fuel cell, which leads to the production of water and oxygen consumption, takes place inside the catalyst layer. In practice, the amounts of water production and oxygen consumption in different areas of the catalyst layer is not constant and have a direct relationship with the amount of current density produced in the catalyst layer, which is obtained from the Faraday relation. Since the channel is not a porous medium and there is no mass source in it, the continuity equation in the channel area is simpler (although the gas diffusion layer is a porous medium, there is no mass source in that area because no chemical reaction occurs).

The momentum equation is generally in the form expressed as follows (Babay et al. 2024a; Kone et al. 2018):

$$\nabla \cdot (\rho \epsilon \vec{u} \vec{u}) = -\epsilon \nabla P + \nabla \cdot (\epsilon \mu^{eff} \nabla \vec{u}) + f_b + S_u \tag{5}$$

In Eq. (5), S_u represents source term, P represents pressure, μ^{eff} represents effective viscosity, and f_b represents volumetric force. Considering the continuity equation and the momentum equation, at the inlet of the gas channels, the boundary condition of the mass flow rate is used. At the outlet of gas channels, the pressure outlet is used. The interior boundary condition is used to communicate with the internal parts of the fuel cell. For initial conditions, the temperature is assumed to be 353 K and the gauge pressure to be 0 Pa. The equation of chemical components is generally expressed as follows (Kone et al. 2018),

$$\nabla \cdot (\epsilon \vec{u} c_k) = \nabla \cdot (D_k^{eff} \nabla c_k) + S_k \tag{6}$$

In Eq. (6), S_k represents the source term, c_k represents the mass fraction, and D_k^{eff} represents the diffusion coefficient. In general, the index k represents the k^{th} component of the

chemical reaction. The Faraday equation in the catalyst layer of the PEM fuel cell is expressed as follows,

$$\dot{n}_{O_2} = -\frac{I}{4F}, \dot{n}_{H_2O} = \frac{I}{2F} \tag{7}$$

In Eq. (7), F shows the Faraday constant, I indicates the generated electric current in the catalyst layer, and

\dot{n}

represents the number of moles of oxygen and water. In the catalyst layer, there is the expression for the source of the components, the value of which can be obtained according to the Faraday constant and the electric current produced. Therefore, it can be written as follows,

$$\begin{cases} \dot{n}_{O_1} = -\frac{I}{4F}, I = i \times A_{effective}, \dot{m}_{O_2} = M_{O_2} \dot{n}_{O_2} \\ S_{O_2} = -\frac{\dot{m}_{O_2}}{V_{cl}}, V_d = A_{effective} \times h_{cl} \end{cases} \Rightarrow S_{O_2} = -\frac{M_{O_2} i}{4F \times h_{cl}} \tag{8}$$

Equation (8) expresses the relationship between the oxygen consumption in the cathode electrode and the generated current density. A negative sign indicates oxygen consumption in the catalyst layer. M_{O_2} represents the mass of a mole of oxygen, h_{cl} indicates the height of the catalyst layer, and i represents the output current density. If, like oxygen for water, the necessary simplifications are made, the relationship between water production at the cathode side and the current density generated in the catalyst layer results from Eq. (9). It should be noted that the positive sign indicates the water production in the catalyst layer.

$$S_{H_2O} = \frac{M_{H_2O} i}{2F \times h_{cl}} \tag{9}$$

The energy equation is generally for the porous medium in the form of Eq. (10). Each component of the phrase related to the energy source is shown in Eq. (11) [37,38]:

$$\nabla \cdot (\epsilon \rho C_p \vec{u} T) = \nabla \cdot (k_{eff} \cdot \nabla T) + S_p^{energy} \tag{10}$$

$$S_u^{energy} = S_u^0 + S_u^{act} + S_u^{DR} + S_u^{evap} \tag{11}$$

The charge equation is in the form of Eq. (12), and the source term due to the production of electric charge in the catalyst is expressed as follows (Babay et al. 2021, 2024a):

$$\nabla \cdot (\sigma \nabla \Phi) = S_u^\phi \tag{12}$$

$$S_u^\Phi = \begin{cases} +j & \text{Anode catalyst} \\ -j & \text{Cathode catalyst} \\ 0 & \text{other location} \end{cases} \tag{13}$$

The Butler-Volmer equation expresses the relationship between the operating voltage and the current density of the fuel cell so that according to the physical characteristics and operating conditions, the amount of operating voltage at any current density can be determined. The Butler-Volmer equation is expressed as follows (Baca et al. 2008):

$$V_{cdl} = V_{rev} - \frac{RT}{\alpha_r F} \ln \left(\frac{i/C_g^{O_2}}{i_0/C_{ref}^{O_2}} \right) - \sigma i \quad (14)$$

In Eq. (18), V_{coll} represents the operating voltage, V_{rv} represents the reversible voltage, α_c represents the cathode charge coefficient, and i_0 is the current density after which the voltage drop starts and its value is constant. $C_{ref}^{O_2}$ represents the oxygen concentration in standard conditions (temperature of 25°C and pressure of 1 atm), $C_g^{O_2}$ represents oxygen concentration in fuel cell operating conditions. Also, σ represents the specific surface resistance. Since in the fuel cell, an electric current is generated in the catalyst layer, the Butler-Volmer equation is established in this region and the generated current is zero in the GDL and inside the channels.

The useful work of a fuel cell is only obtained when a current is drawn, but the actual potential of the cell (E_{cell}) is decreased relative to its thermodynamic equilibrium potential (E) due to irreversible losses. The cell potential is obtained by subtracting all the overpotentials (losses) from the thermodynamic equilibrium potential with the following expression:

$$E_{cell} = E - \eta_{ohm} - \eta_{mem} - \eta_{Diff} \quad (15)$$

The equilibrium potential is determined using the Nernst equation:

$$E_{cell} = E - \eta_{ohm} - \eta_{mem} - \eta_{Diff} \\ E = 1.229 - 0.83 * 10^{-3}(T - 298) + 4.3085 \\ * 10^{-5}T * [\ln P_{H_2} \frac{1}{2} \ln P_{O_2}] \quad (16)$$

The anode and cathode activation overpotentials are calculated from the Butler-Volmer equation (Eqs. (21) and (22)). The current densities are calculated as follows, on the anode side:

$$i_a = i_a^0 \left(\frac{C_{H_2}}{C_{ref}^{H_2}} \right)^{0.5} \left[\exp\left(\frac{\alpha_a F}{RT} \eta_a\right) - \exp\left(\frac{\alpha_c F}{RT} \eta_a\right) \right] \quad (17)$$

And on the cathode side:

$$i_c = i_c^0 \left(\frac{C_{H_2}}{C_{ref}^{H_2}} \right)^{0.5} \left[\exp\left(\frac{\alpha_a F}{RT} \eta_c\right) - \exp\left(\frac{\alpha_c F}{RT} \eta_c\right) \right] \quad (18)$$

where:

α_a and α_c are the two charge transfer coefficients, and C_{H_2} and C_{O_2} are the hydrogen and oxygen concentrations at the membrane/electrode interfaces. They are calculated by Henry's law:

$$C_{H_2} = \frac{P_a X_{H_2}}{K_{H_2}} \quad (19)$$

$$C_{O_2} = \frac{P_c X_{O_2}}{K_{O_2}} \quad (20)$$

K_{H_2} and K_{O_2} being Henry's constants for hydrogen and oxygen. In Eqs. (21) and (22), the activation overpotentials $\eta_{a,c}$ are determined from the local potentials of the electrodes and the membrane:

$$\eta_{a,c} = \varphi_{a,c} - \varphi_m - E_{a,c}^{eq} C_{H_2} = \frac{P_a X_{H_2}}{K_{H_2}} \quad (21)$$

With $E_{a,c}^{eq}$ the equilibrium potentials of the anode and cathode. The equilibrium potential of the anode is zero, and that of the cathode depends on the battery temperature (in Kelvin) according to the expression:

$$E_{a,c}^{eq} = 1.23 - 0.83 * 10^{-3}(T - 298) \quad (22)$$

3 Simulation model

The system is governed by a set of boundary conditions designed to ensure its smooth operation: • Internal boundaries maintain continuity. • Channel walls enforce a no-slip condition, optimizing fluid dynamics. • Initial values across the system are uniformly set to zero for consistent starting conditions. • The channel outlet experiences no backpressure, benefitting from convective flux boundary conditions. • Both the inlet and outlet have their outer edges constrained to zero for stability. • Electrically, bipolar plates on either side of the cell are grounded and aligned with the operational potential. • Remains insulated, securing its performance from external environmental influences.

The analysis delved into key considerations, such as regulating reactant gas flow at outlets by adjusting pressure and implementing mass flow inlets at entrances. Sealed plates enveloped the gas diffusion layer (GDL) and catalyst layer at both inlet and outlet points, ensuring a no-slip velocity condition and preventing species mass transfer. To address crossover and pressure-related issues, the membrane-electrode interface was treated as a wall. Anode and cathode terminals maintained a constant reference voltage of zero,

with inlet boundary conditions predetermined based on stoichiometric flow rate, temperature, and mass fraction.

The Dirichlet condition is used at the inlet of the cathodic and anodic channels for the species, heat and mass conservation equations. The mass flow rates are considered constant at each channel inlet in all cases of the realized simulations (Table 3).

In Fluent CFD, the software's momentum equation solver employed a pressure correction technique to handle varying pressures in different gas channels, with pressure conditions applied at the outlets. The ionic potential in the membrane was set to zero at the anode-side interface, while the cathode-side interface received a designated negative flux representing proton consumption. Water flux was determined from the gradient of the chemical potential, assuming equilibrium between water in the membrane and water vapor in the electrode. This study utilized a mathematical model in ANSYS Fluent to analyze PEMFC cells, with computational areas designated as porous, excluding current collectors and wall

terminals. Computational domains were created using ANSYS Design Modeler and ANSYS Meshing, laying the foundation for comprehensive simulations.

In addition, for the serpentine Flow-Field PEM-FC, ANSYS Fluent provides a comprehensive mesh quality analysis. The skewness of mesh elements is well within desirable parameters, with an average angle of approximately 0.31095. The maximum skewness angle, at around 0.91685, is also acceptable, as values close to zero or less than 1 are preferred to prevent excessive distortion of elements. The standard deviation, measuring the spread of skewness angles around the average, is 0.18663, indicating a reasonably uniform distribution. In terms of mesh statistics, the simulation involves 220,361 nodes and 802,283 elements, highlighting a well-balanced mesh with satisfactory skewness angles. This aspect is crucial for ensuring the accuracy of numerical simulations. While these results offer an overall understanding of mesh quality, a more detailed evaluation may be necessary depending on the specific requirements of the simulated problem Fig. 2. In contrast, for the straight channel PEM-FC, the mesh consists of 28,548 nodes and 25,200 elements. This configuration ensures a solid foundation for accurate simulations in Fig. 3.

Table 3 Operation parameters for the straight channel fuel cell section

Parameter	Value	Unit
Inlet temperature, anode and cathode	80	°C
Anode side pressure	2	atm
Cathode side pressure	2	atm
Anode stoichiometric flow rate	3	–
Cathode stoichiometric flow rate	3	–
Relative humidity of inlet gases	100	%
Oxygen/nitrogen ratio	0.21/0.79	–

4 Results and discussion

The passage examines the validation of model results under standard operating conditions by comparing them with experimental data from Wang et al. (Wang et al. 2003). Figure 4 illustrates a close match between the computed and experimental polarization curves, indicating satisfactory agreement between the model and experimental outcomes.

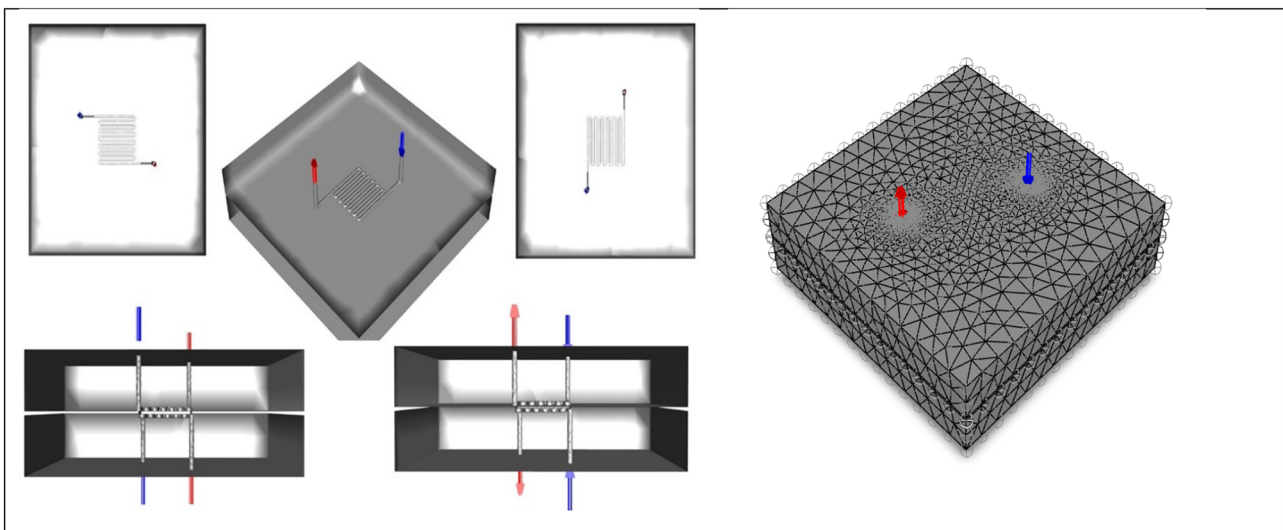


Fig. 2 Diagram of a Serpentine Flow-Field PEM-FC

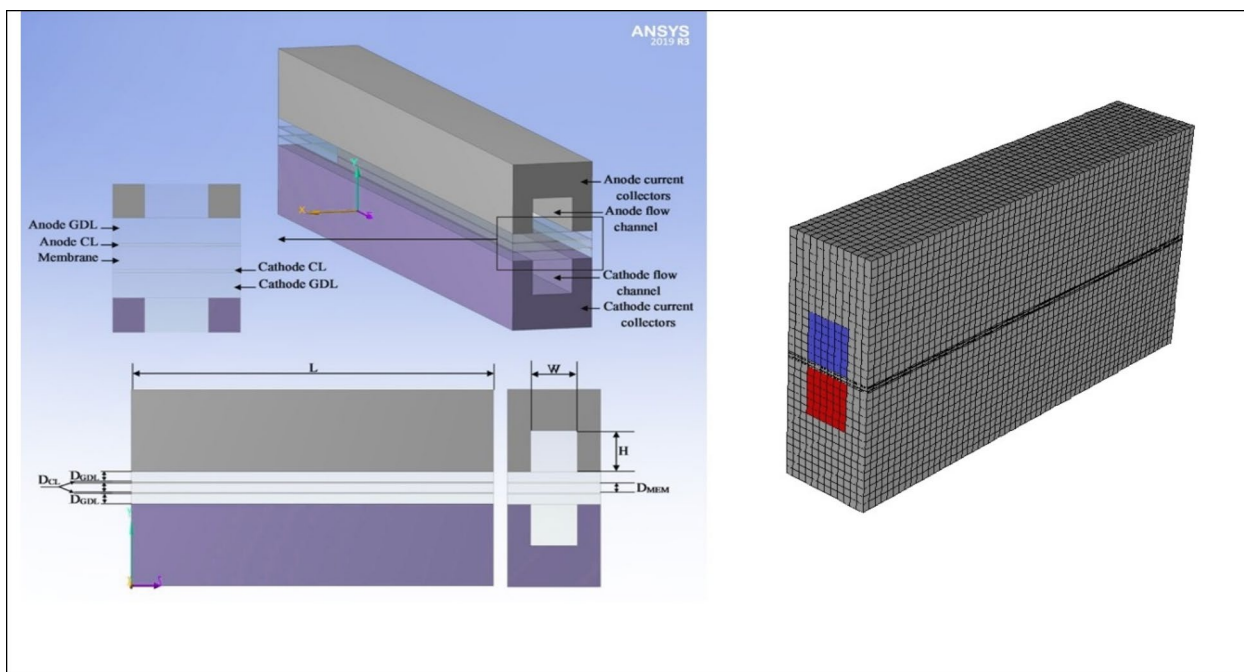


Fig. 3 Diagram of a Straight channel PEM-FC

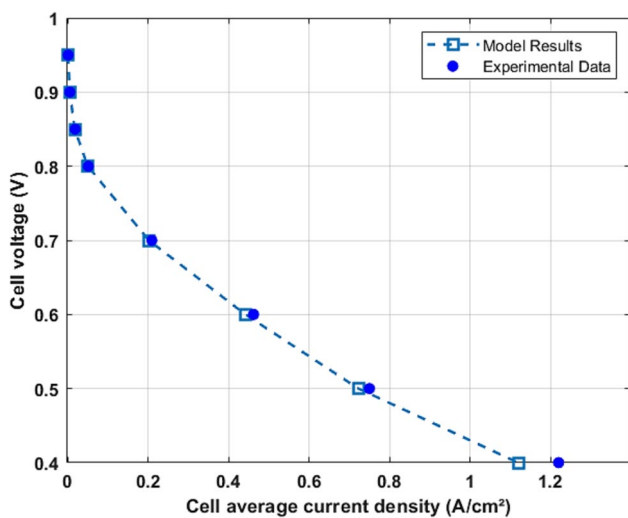


Fig. 4 PEM-Fuel cell polarization curve validation

Nonetheless, a discrepancy arises in the model’s cell current densities within the mass transport-limited region (1.2 A/cm²), surpassing the corresponding experimental values. This deviation stems from a common limitation found in single-phase models, which struggle to accurately address reduced oxygen transport due to water flooding at the cathode during high current density periods. Additionally, anode drying contributes to the observed performance decrease at elevated current density. To deepen understanding of the fuel cell’s performance and identify crucial parameters, the

study conducts parametric studies, varying specific parameters while maintaining others constant. These investigations are expected to shed light on key factors influencing fuel cell performance. Emphasis is placed on exploring diverse operating conditions to comprehensively evaluate the fuel cell’s behavior, particularly at a nominal current density of 1 A/cm², with further insights promised in subsequent sections.

4.1 Effet des températures de fonctionnement

Figure 5 shows that the fuel cell performance increases with the increase in cell temperature from 50°C to 80°C. The exchange current density increases with the rise in fuel cell temperature, reducing activation losses. This could explain the performance improvement. The polarization curve for the fuel cell temperature at 80°C is lower than the other curves in the low current density region. When the fuel cell temperature is maintained at 80°C, higher than the 70°C humidification temperature, at low current densities, the membrane material in the catalytic layer may not be fully hydrated. This could result in a decrease in the active surface of the catalyst. With the increase in current density, the water production rate increases proportionally. Higher rates of water production at higher current densities keep the membrane material in the catalytic layer better hydrated, leading to an increase in the active surface of the catalytic layers and improving fuel cell performance. It is observed in the figure that the fuel cell current density limit increases as the cell temperature rises from 50°C to 80°C, indicating

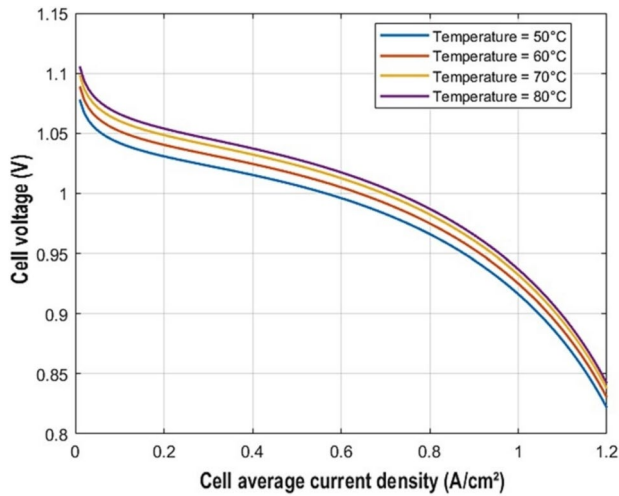


Fig. 5 Polarization curves for different fuel cell temperatures

an improvement in mass transport due to the increase in diffusivity with temperature. The shifting of the polarization curves towards higher voltages at higher current densities with the increase in cell temperature is also attributed to the increase in membrane conductivity.

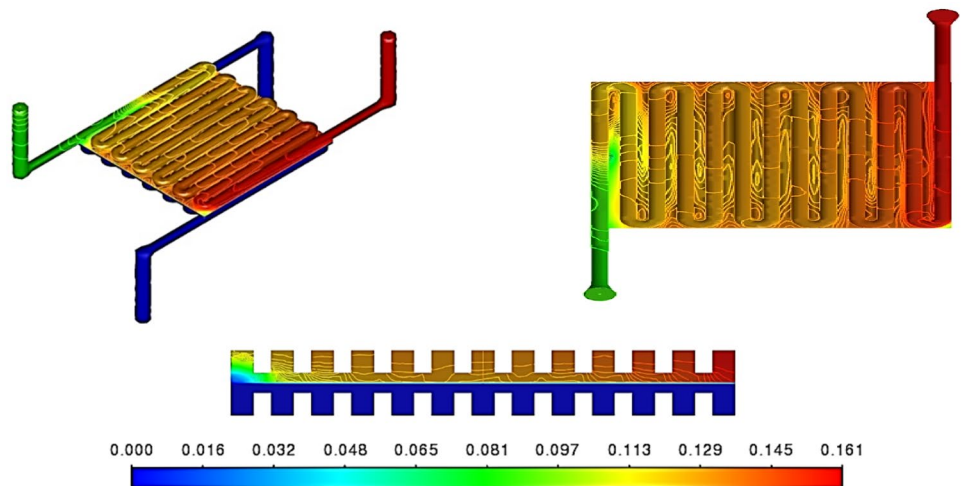
4.2 Profiles of reactant and product concentrations

4.2.1 Distributions of oxygen concentration fractions

Figure 6 illustrates the profound impact of serpentine flow channels in fuel cells. As oxygen traverses from the gas channel to the gas diffuser, its concentration experiences a steady decline, influenced by diffusion through various constituents such as nitrogen, reaction water, and the catalyst layer. This reduction is quantified by a decrease in concentration, reaching as high as 17% from the gas diffuser

to the catalyst layer interface. The presence of a rib within the channel further amplifies oxygen’s diffusion resistance, resulting in a notable decrease in concentration at the interface by approximately 12%. Additionally, oxygen consumption along the channels contributes to its gradual depletion, with a decrease of 15% observed from the inlet to the outlet. At low current density, characterized by a sluggish reaction rate and minimal oxygen demand, the oxygen concentration remains uniformly distributed. This uniformity ensures a steady diffusion rate, with only a marginal change in concentration observed from the gas channels to the gas diffuser. However, at high current density, where the rapid reaction rate outpaces oxygen supply from diffusion, there is a significant decrease in the concentration fraction at the outlet gas channel. This decline is particularly pronounced, with a reduction of approximately 20% observed from the bottom to the top, driven by the flow of velocity vectors. Consequently, higher concentrations, exceeding 10%, are observed at the bottom due to channel geometry. In fuel cells employing humidified air, the limiting current density is predominantly governed by cathode conditions, given oxygen’s lower diffusivity compared to hydrogen. The maintenance of oxygen concentration equilibrium at the catalyst layer relies on a delicate balance between consumption and diffusion, with a notable reduction of 10% observed in oxygen concentration at the catalyst layer interface. Transitioning to Fig. 7, it offers a graphical depiction of the molar fraction distribution of oxygen in the cathode channel, Gas Diffusion Layer (GDL), and cathode catalyst layer. At medium current density, oxygen consumption occurs gradually, with minimal diffusion limitations. However, at high current density, the oxygen concentration beneath the land areas reaches its minimum value of zero, causing no further decrease. The molar concentration of oxygen gradually reduces by 17% from the inlet to the outlet of the channel, indicative of progressive utilization along the flow path. Moreover, the decline in molar

Fig. 6 Cross-section contours Oxygen molar fraction distribution in the PEMFC in serpentine flow plate



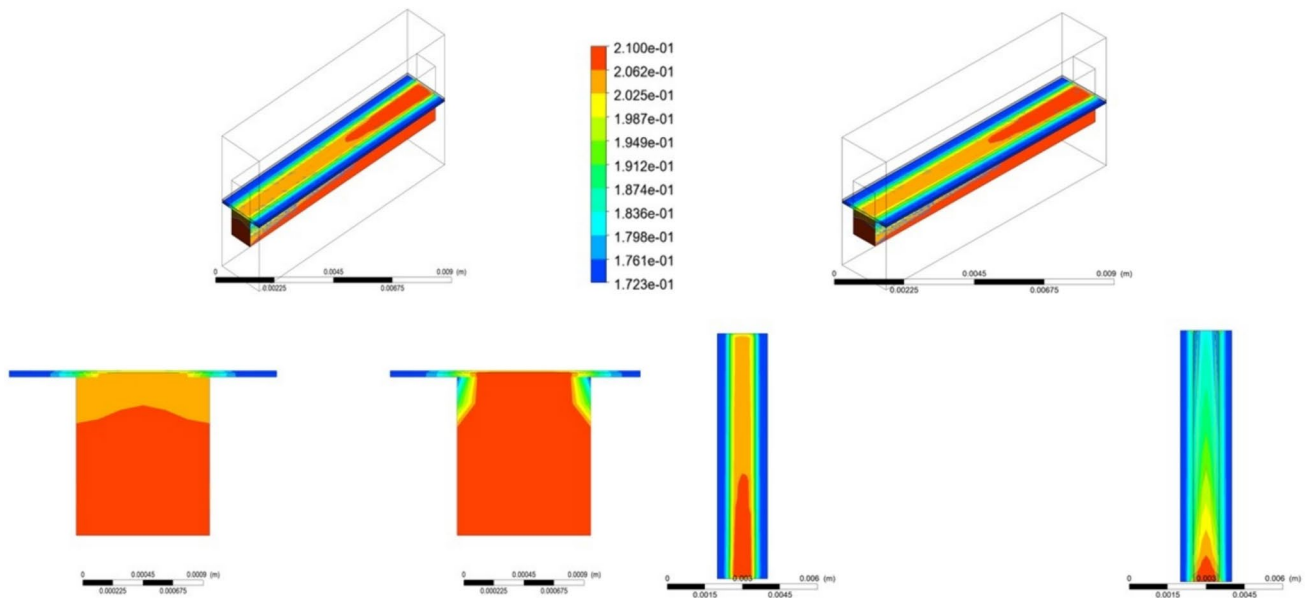


Fig. 7 Distribution of Oxygen Molar Fraction in the Cathode Channel, Gas Diffusion Layer, and Cathode Catalyst Layer- with straight flow field channels

hydrogen concentration in the anodic diffusion layer surpasses the decrease in oxygen concentration in the cathodic GDL, underscoring the intricate interplay between reactant consumption and distribution within the fuel cell.

4.2.2 Distributions of hydrogen concentration fractions

Figure 8 illustrates the intricate distribution of hydrogen molar fraction within the PEMFC, employing serpentine flow plate channels. This visualization offers a nuanced understanding of how hydrogen concentration varies spatially across the fuel cell system. The contour plot vividly portrays substantial fluctuations in hydrogen concentration along the cathode channel, representing a percentage variation range from 0 to 90%.

Analyzing these results in the context of existing literature, several studies have emphasized the critical role of channel design in influencing oxygen concentration gradients within fuel cell systems. For instance, research by Scholta et al. (Scholta et al. 2006) investigated the impact of channel geometry on reactant distribution and performance in PEMFCs. Their findings underscored the significance of optimizing channel configurations to achieve uniform reactant distribution and enhance overall cell performance. Similarly (Babay et al. 2024a) highlighted the importance of considering flow field designs in fuel cell systems, particularly in managing reactant distribution and minimizing concentration gradients.

In Fig. 9, which depicts the hydrogen molar fraction distribution in the anode channel, GDL, and anode catalyst

layer with straight flow field channels, we observe significant fluctuations in oxygen concentration dynamics, with a variation ranging from 40 to 61%. These results align with previous studies by Johnson et al. (cite), who investigated the influence of channel architecture on reactant distribution and performance in PEMFCs. Their research emphasized the role of flow field design in optimizing reactant distribution and minimizing concentration variations across the cell. Under medium current density conditions, oxygen consumption occurs gradually without diffusion limitations. However, at high current density, the oxygen concentration beneath the land areas reaches a minimum value of zero, indicating the onset of diffusion limitations. This finding is consistent with prior research by Kone et al. (Kone et al. 2018), who studied the effects of current density on reactant distribution and performance in PEMFCs. Their results highlighted the importance of managing oxygen distribution to mitigate concentration gradients and improve cell efficiency. Rostami et al. (Rostami and P. Mohamad Gholy Nejad, A. Vatani 2016) studied a 3-D to understand the influence of bending size on a PEM fuel cells. The findings show that increasing the bend from 1 mm to 1.2 mm, not only significantly reduces the overvoltage, but also reduces the temperature gradient. A review of research on flow simulation in PEM fuel cells with different channel shapes shows that the common denominator of all this research is that most of them focus only on the cathode side of the PEM fuel cell and the different cross-sections. In summary, our findings underscore the intricate interplay between channel design, oxygen distribution, and fuel cell performance. By elucidating

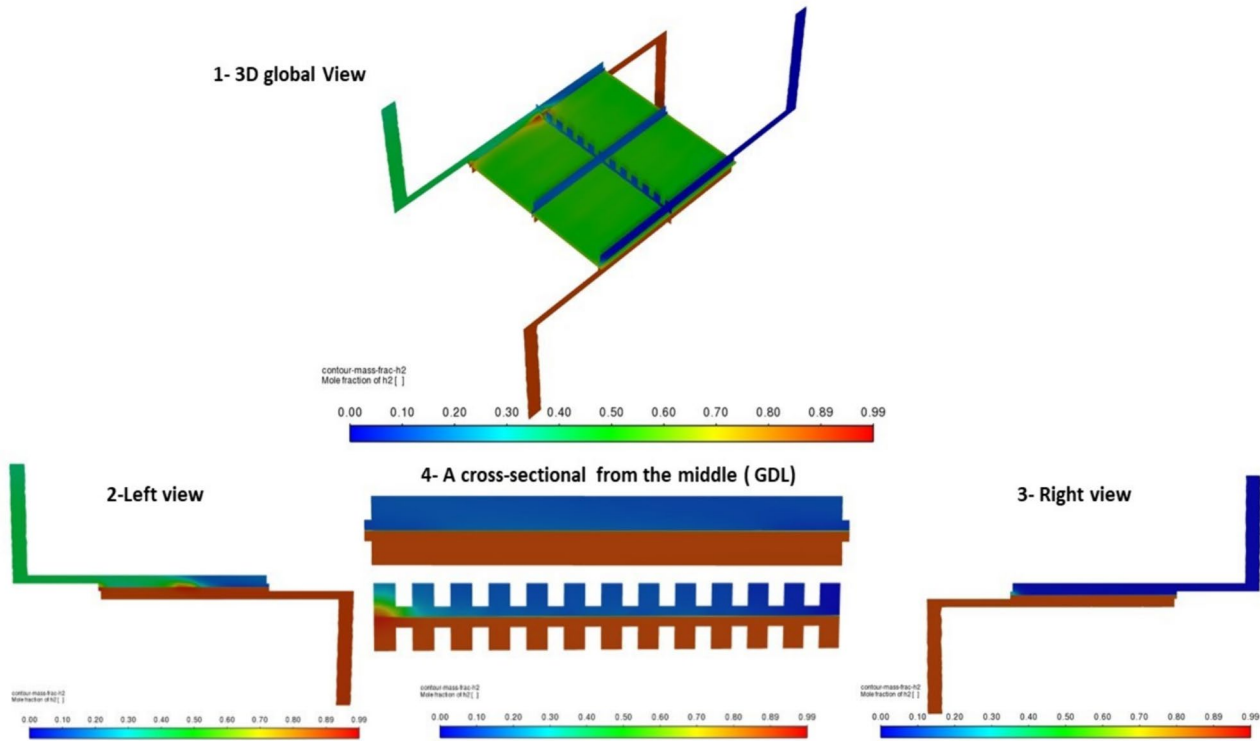


Fig. 8 Cross-section contours Hydrogen molar fraction distribution in the PEMFC in serpentine flow plate

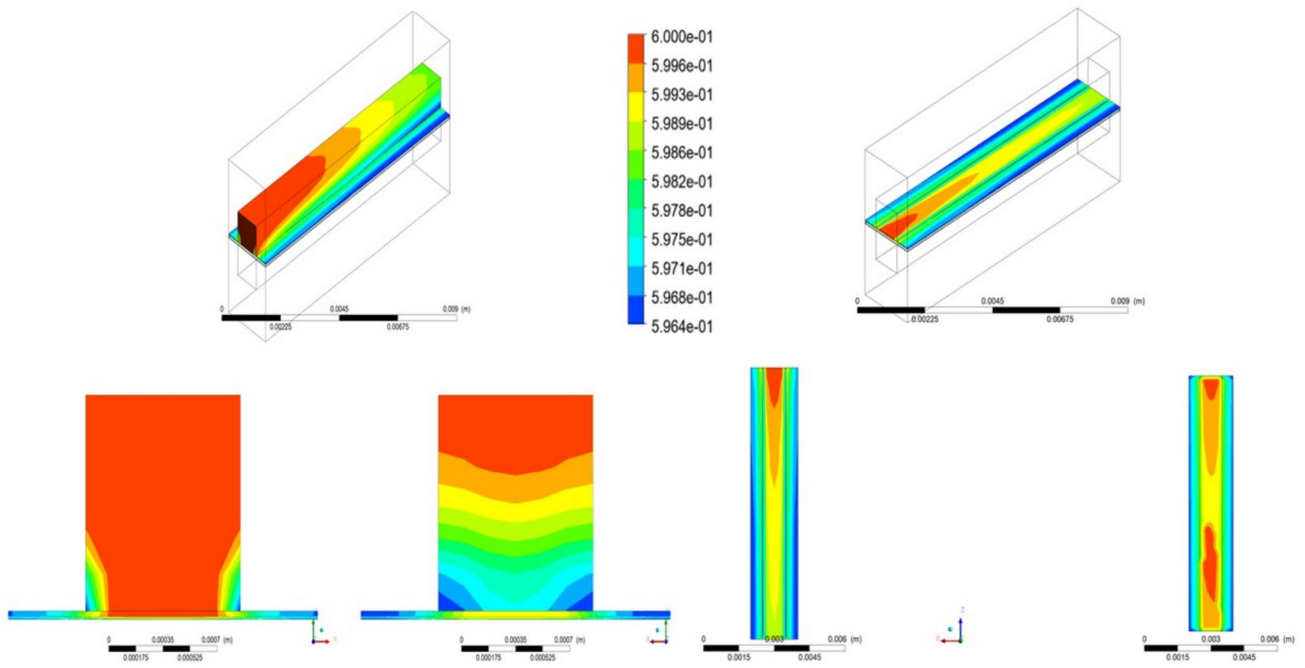


Fig. 9 Hydrogen molar fraction distribution in the anode channel and GDL and the anode catalyst layer with straight flow field channels

these dynamics, we contribute to a deeper understanding of how channel configurations influence reactant distribution and overall cell performance. These insights can inform the development of optimized channel designs and operational strategies aimed at enhancing fuel cell efficiency and durability in real-world applications.

4.3 Velocity distributions

Figure 10 and Fig. 11 provide detailed insights into the velocity distribution within different flow field channel designs in PEM fuel cells. In Fig. 10, which illustrates velocity contours in straight flow field channels, the variation ranges from 0 to 4.043×10^{-3} . This range highlights the intricate dynamics governing gas flow within these channels. The velocity distribution is influenced by factors such as channel width, height, flow rate, and pressure drop across the cell. Straight channel designs offer advantages like higher power output and lower pressure drop but present challenges in controlling velocity distribution compared to serpentine flow-field designs. Moving to Fig. 11, which presents velocity contours in a serpentine flow channel PEM fuel cell, the variation spans from 0 to 3.63. Serpentine flow channels consist of interconnected, U-shaped channels that alternate in direction. This design promotes a more uniform velocity distribution, crucial for preventing reactant depletion and ensuring optimal performance.

The velocity distribution in serpentine flow channels is affected by parameters like flow rate, channel geometry, and pressure drop. Achieving uniform velocity distribution in these channels requires careful design considerations to maintain consistent flow rates throughout. Comparing velocity distributions between straight and serpentine flow channels provides valuable insights into the advantages and challenges of each design. While straight channels offer benefits like higher power output, achieving uniform velocity distribution can be more challenging. In contrast, serpentine flow channels promote more uniform velocity distribution,

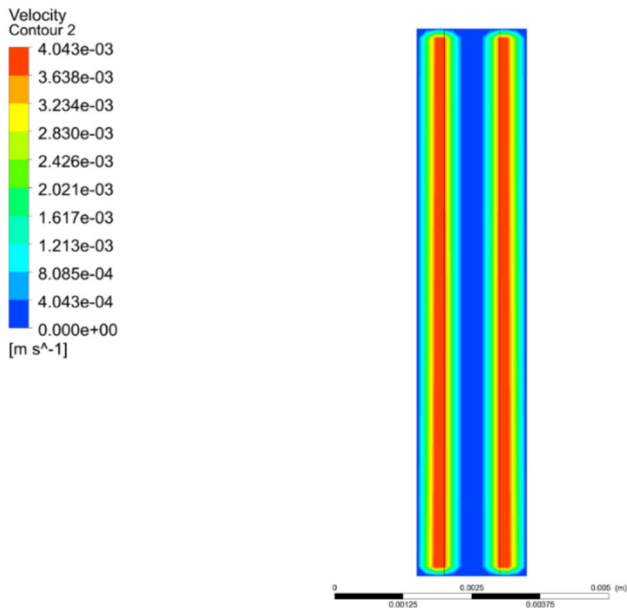


Fig. 10 Cross-section contours of the Velocity contours in straight flow field channels

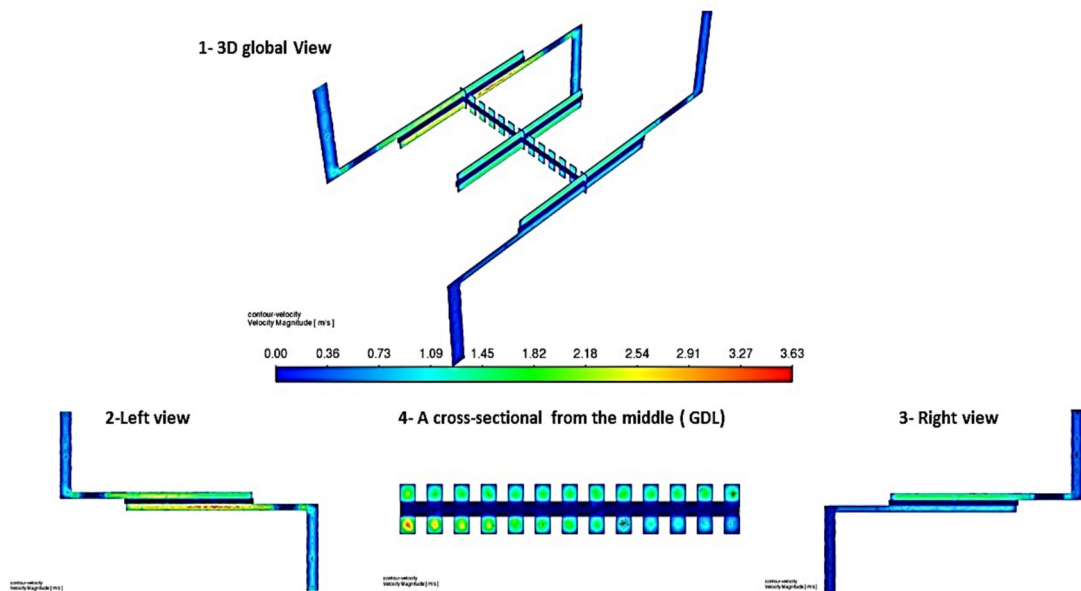


Fig. 11 Cross-section contours of the Velocity contours in a serpentine flow channel

contributing to enhanced fuel cell performance. These findings underscore the importance of optimizing flow channel and diffuser design to achieve uniform velocity distribution, ultimately improving fuel cell efficiency and performance in various applications.

4.4 Temperature, pressure distribution inside the PEM fuel cell

The composition of gases entering a fuel cell is significantly impacted by temperature, as well as the various processes that occur inside the fuel cell. Temperature can affect the level of loading and the level of electrochemical activity, leading to changes in the molar fraction of hydrogen and oxygen. Additionally, the partial pressure of water vapor entering the cell is solely determined by temperature, as long as the incoming gases are fully humidified. At atmospheric pressure, temperature has a more significant impact on the composition of incoming gases compared to higher pressures. Figures 12 and 13 illustrate the temperature distribution within the fuel cell for different current densities. The highest temperature is observed near the inlet of the cathode side, but even with an even distribution of current density, the increase in temperature is only around 1 K for low current densities. The impact of temperature on fuel cell performance is not limited to gas composition, as it also affects the fuel cell's efficiency and durability. High temperatures can lead to accelerated degradation of the fuel cell's materials and reduced performance, while low temperatures can lead to reduced efficiency and slower reaction rates. Proper temperature control is crucial for maintaining optimal fuel cell performance, and various methods are used to achieve this. Cooling systems, such as air or liquid cooling, can be used to manage temperature, as well as insulation and heat exchange systems. Additionally, temperature sensors and control systems are used to monitor and regulate temperature within the fuel cell. In conclusion, temperature plays a crucial role in the composition of gases entering a fuel cell, as well as the efficiency and durability of the fuel cell. Proper temperature control is essential for maintaining optimal performance, and various methods are used to achieve this.

4.5 Distribution of water content in proton exchange membrane

Figure 14 provides a detailed visualization of water content distributions within the membrane of a PEM fuel cell utilizing serpentine flow plate channels. The variation spans from 0.61 to 8.15, showcasing significant heterogeneity in water distribution across the cell. Contrastingly, Fig. 15 illustrates water content distributions in a PEM fuel cell with straight flow field channels, demonstrating a range from 0 to 5. Water content within the PEM membrane

profoundly influences its resistance to proton movement, a critical factor in fuel cell performance. Higher water content corresponds to lower membrane resistance, facilitating enhanced proton conductivity and, consequently, improved fuel cell efficiency. The spatial distribution of water content offers valuable insights into areas of potential resistance buildup and informs effective water management strategies. The observed water content distribution patterns reveal distinct trends along the cathode-to-anode axis. Near the cathode, regions typically exhibit lower water content, resulting in elevated membrane resistance. This phenomenon can be attributed to reduced hydration levels and limited water availability in these areas. In contrast, as one progresses towards the anode, water content increases, leading to the onset of two-phase flow phenomena in the gas channel and diffuser regions. This progression ultimately culminates in complete membrane humidification near the anode, characterized by the lowest resistance to proton movement. The influence of temperature on water content and fuel cell performance is a critical consideration. Elevated stack temperatures tend to reduce membrane hydration and water content, thereby diminishing overall cell performance. This effect is particularly pronounced in regions where water content is crucial for maintaining optimal proton conductivity, leading to uneven current density distributions and compromised cell efficiency. Effective water management strategies are essential for maximizing fuel cell performance and longevity. Previous studies have used the correlation developed by Springer et al. (Görgün et al. 2006) to calculate water content. These strategies encompass various factors, including regulating relative humidity, temperature, and gas flow within the fuel cell system. Common approaches involve external humidification techniques and optimizing cathode porous layers to enhance water retention and transport. Additionally, careful design considerations for flow channels and diffusers play a pivotal role in facilitating the removal of excess water from the fuel cell, thereby preventing flooding and ensuring uniform water distribution. Advanced techniques such as impedance spectroscopy, neutron radiography, and NMR imaging serve as invaluable tools for quantifying and visualizing water content within PEM fuel cells. These techniques enable precise measurement and monitoring of water distribution, allowing for proactive maintenance and optimization of fuel cell operation. In conclusion, understanding the intricate relationship between water content and membrane resistance is paramount for optimizing PEM fuel cell performance. By leveraging advanced measurement techniques and implementing effective water management strategies, we can enhance fuel cell efficiency, durability, and reliability, ultimately advancing the transition towards sustainable energy solutions.

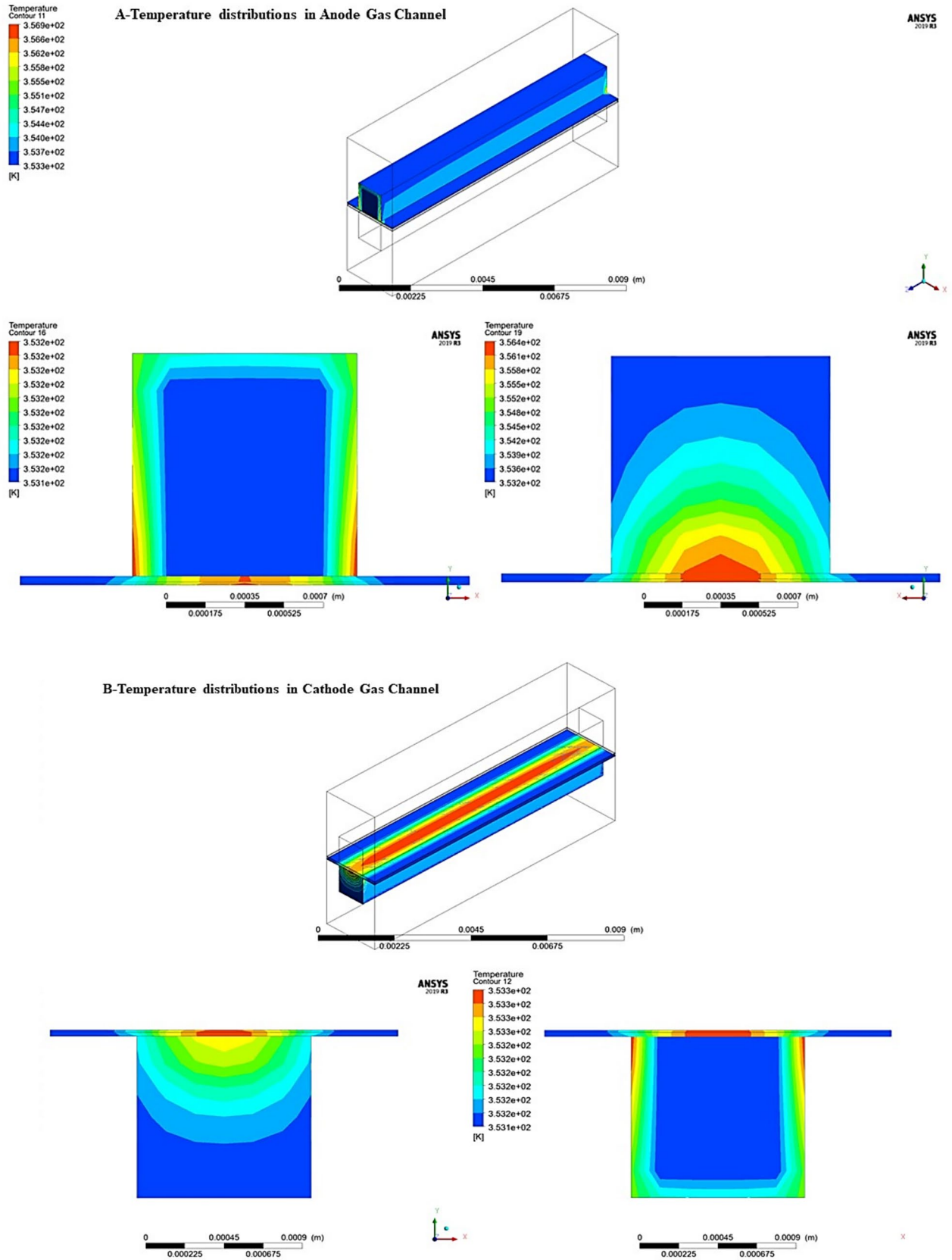


Fig. 12 Temperature distribution a, b inside PEMFC with straight flow field channels

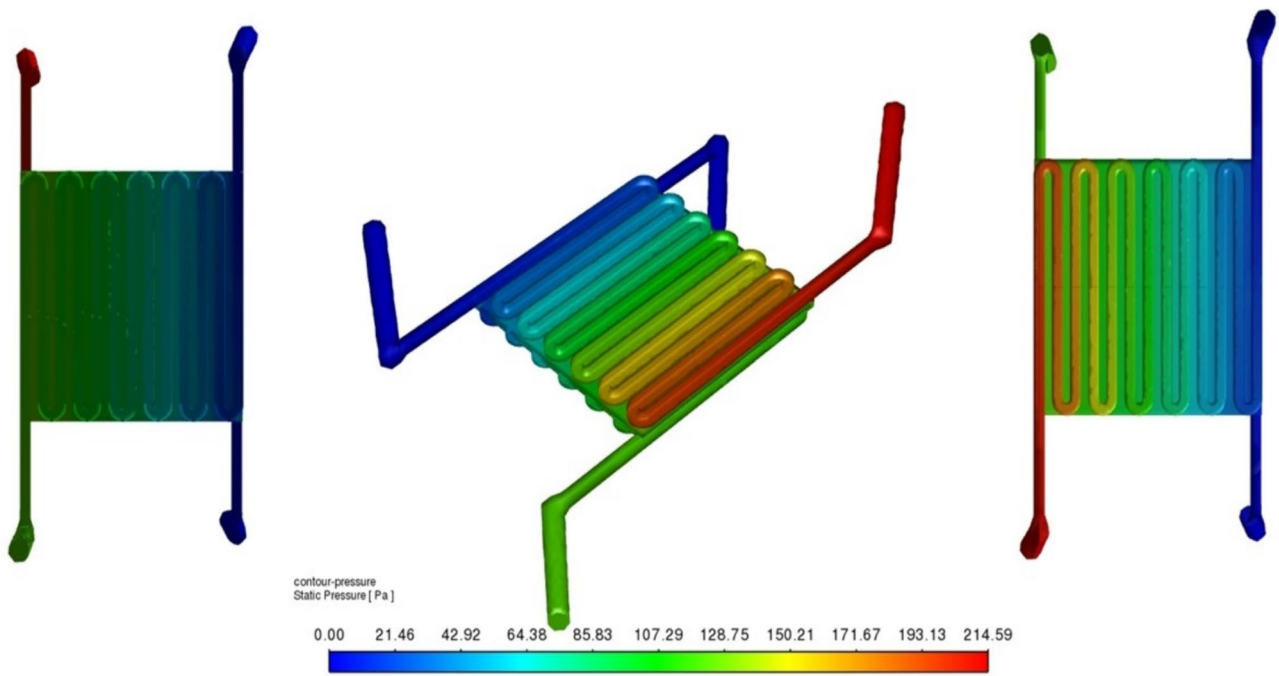


Fig. 13 Pressure distribution inside PEMFC with serpentine flow plate

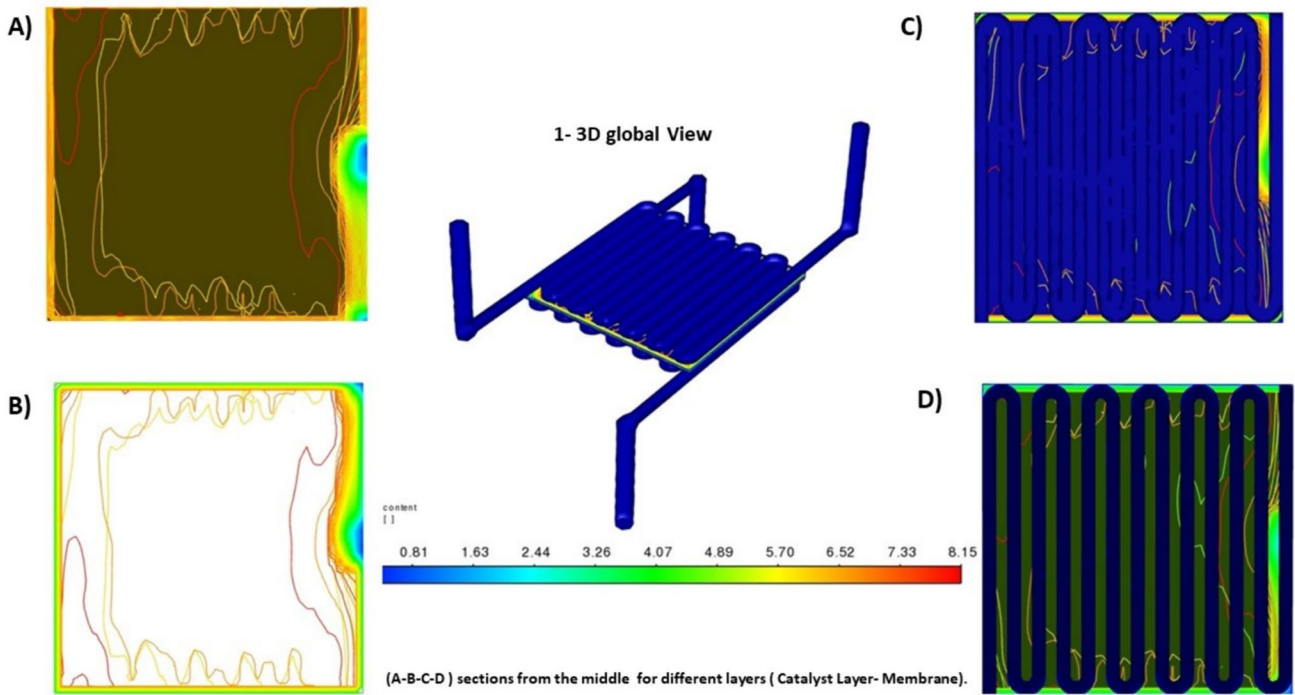


Fig. 14 Water content distributions in the membrane of a PEM fuel cell in serpentine flow plate

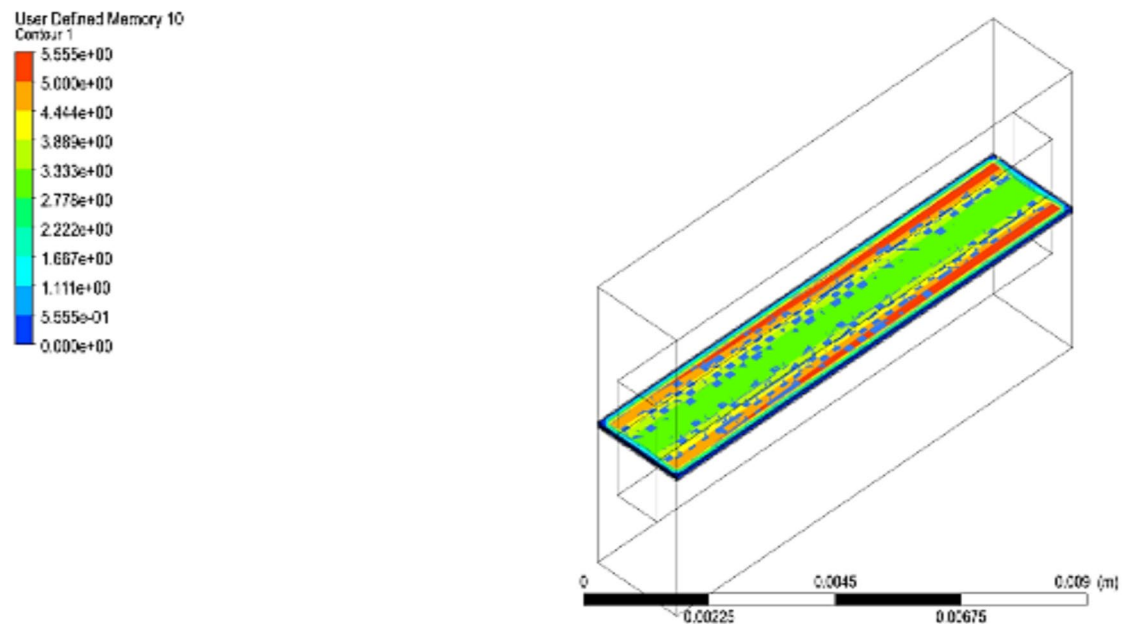


Fig. 15 Water content distributions in the membrane of a PEM fuel cell with straight flow field channels

4.6 Advancing proton exchange membrane fuel cells: technological and economical feasibility analysis

In this comprehensive study, we embark on an in-depth exploration of the technological and economical feasibility of advanced Proton Exchange Membrane (PEM) fuel cell designs. Our analysis is structured into five meticulously crafted subsections, each delving into critical aspects pivotal for assessing the viability of these innovative fuel cell configurations.

For instance, when examining the practical limitations in scaling up the proposed methodologies, we encountered challenges related to material availability. Certain rare earth metals critical for fuel cell component fabrication may face supply chain constraints, potentially hindering large-scale production. Additionally, the complexity of manufacturing processes, such as intricate electrode assembly procedures, poses challenges for mass production. Addressing these technological constraints requires innovative solutions in material sourcing and manufacturing automation to ensure scalability without compromising performance.

During our critical evaluation of computational models, we identified instances where simplifying assumptions led to discrepancies between simulated and real-world performance. For example, while computational fluid dynamics (CFD) models provide valuable insights into fluid flow behavior within fuel cells, their accuracy may be compromised by oversimplified boundary conditions. By transparently acknowledging these limitations and validating model outputs against experimental data, we enhance the reliability of our analyses and facilitate informed decision-making.

Through meticulous analysis of efficiency metrics, we uncovered intriguing insights into the energy performance landscape of advanced PEM fuel cell designs. For instance, simulations revealed that novel catalyst formulations significantly enhance power output under high current density conditions, thereby improving overall energy conversion efficiency. Moreover, operational stability profiles derived from experimental data demonstrated the robustness of these designs in prolonged operation, further bolstering their appeal for real-world applications.

By conducting a comprehensive comparison of physico-chemical characteristics, we uncovered compelling advantages inherent in each fuel cell design. For instance, while serpentine flow plate configurations excel in promoting uniform reactant distribution, straight flow field channels offer superior gas diffusion properties, enhancing overall cell performance. Moreover, detailed analyses of reaction kinetics highlighted the catalytic efficiency of specific electrode materials, shedding light on opportunities for further optimization.

In assessing the feasibility of large-scale industrial manufacturing, we analyzed key cost drivers and market dynamics influencing the commercialization potential of advanced PEM fuel cell technologies. For instance, a detailed cost-benefit analysis revealed that while initial investment costs for implementing novel manufacturing processes may be substantial, long-term operational savings and market competitiveness justify these expenditures. Furthermore, strategic partnerships with industry leaders and proactive engagement with regulatory bodies can expedite market entry and drive widespread adoption.

Through this comprehensive analysis, we aim to provide stakeholders, policymakers, and researchers with a holistic understanding of the opportunities and challenges associated with the adoption of advanced PEM fuel cell technologies. By addressing key technological, economical, and performance-related considerations, we pave the way for accelerating the transition towards a sustainable energy future powered by innovative fuel cell technologies.

5 Conclusions

In summary, the innovative model developed in this study provides a comprehensive representation of species transport and reactions in various parts of the PEM fuel cell, including the impact of ribs on species transport and the movement of species in the anode and cathode gas channels. The study showed that using the same stoichiometric flow ratio for the oxidant in a 2D, single-phase model consistently overestimates fuel cell efficiency. It also revealed that a straight flow field channel performs worse than a serpentine flow-field when no water is added to humidify the cathode inlet air. Furthermore, the distribution of current density in the fuel cell changes with changes in loading conditions, with the maximum current density shifting towards the center of the channel as the load increases. Overall, this innovative model provides a more accurate prediction of fuel cell performance and emphasizes the importance of considering multiple factors, including flow field design and changes in loading conditions, in determining fuel cell efficiency. These findings can guide the development of future PEM fuel cell designs and promote sustainable energy solutions. The study provides valuable insights into the sustainability of Serpentine Flow-Field and Straight channel PEM fuel cells through numerical analysis, with the former having higher efficiency and durability and the latter being more cost-effective. Freire et al. (Freire et al. 2014) studied the operational parameters on the performance of PEMFCs having different (rectangular and trapezoidal) cross-section shape. Their results showed that the trapezoidal channel has a high ability to remove water from the cathode. However, recent experimental studies show that for certain operating conditions, overflow can occur in the anode gas channels and can be even more noticeable than on the cathode side (Lee and Bae 2012). A literature review shows that robust studies have been performed in relation to fuel cell simulations. However, most.

studies focus on the study of physical parameters (relative humidity, cell voltage, stoichiometric ratio, mass flow rate, etc.) and their impact on fuel cell performance.

Acknowledgements None.

Author's contribution MAB: Conceptualization, Data curation, Formal analysis, Investigation, Methodology, Software, Validation, Visualization, Writing—original draft, Writing—review and editing. MA: Methodology, Validation, Visualization, Writing—review and editing. AC: Investigation, Project administration, Supervision, Validation. MM: Methodology, Project administration, Resources, Supervision, Validation, Visualization.

Funding This study and all authors have received no funding.

Declarations

Conflict of interest The authors have no conflicts of interest to declare.

Research involving human participants and/or animals None.

Informed consent None.

References

- Ahmed DH, Sung HJ (2008) Design of a deflected membrane electrode assembly for PEMFCs. *Int J Heat Mass Transf* 51:5443–5453. <https://doi.org/10.1016/j.ijheatmasstransfer.2007.08.037>
- Ahsan N, Al Rashid A, Zaidi AA, Imran R, Abdul Qadir S (2021) Performance analysis of hydrogen fuel cell with two-stage turbo compressor for automotive applications. *Energy Rep* 7:2635–2646. <https://doi.org/10.1016/j.egy.2021.05.007>
- Babay MA, Adar M, Mabrouki M v Modeling and simulation of a PEMFC using three-dimensional multi-phase computational fluid dynamics model. *Proc 2021 9th Int Renew Sustain Energy Conf IRSEC 2021*. <https://doi.org/10.1109/IRSEC53969.2021.9741144>
- Babay MA, Adar M, Chebak A, Mabrouki M (2023) Dynamics of gas generation in porous electrode alkaline electrolysis cells: an investigation and optimization using machine learning. *Energies* 16:5365. <https://doi.org/10.3390/EN16145365>
- Babay M-A, Adar M, Chebak A, Mabrouki M (2024a) Exploring the sustainability of serpentine flow-field fuel cell, straight channel PEM fuel cells high temperature through numerical analysis. *Energy Nexus*, p 100283. <https://doi.org/10.1016/j.nexus.2024.100283>
- Babay MA, Adar M, Nouri R, Chebak A, Mabrouki M (2024b) Integrated thermodynamic analysis and channel variation effects on solid oxide electrolysis for efficient hydrogen generation. *Procedia Comput Sci* 236:152–159. <https://doi.org/10.1016/j.procs.2024.05.016>
- Babay MA, Adar M, Touairi S, Chebak A, Mabrouki M (2024c) Numerical simulation and thermal analysis of pressurized hydrogen vehicle cylinders: impact of geometry and phase change materials. *J Adv Res Fluid Mech Therm Sci*. 117(2), 71–90. <https://doi.org/10.37934/arfmts.117.2.7190>
- Baca CM, Travis R, Bang M (2008) Three-dimensional, single-phase, non-isothermal CFD model of a PEM fuel cell. *J Power Sources* 178:269–281. <https://doi.org/10.1016/j.jpowsour.2007.12.023>
- Barnoon P, Toghraie D, Mehmandoust B, Fazilati MA, Eftekhari SA (2022) Natural-forced cooling and Monte-Carlo multi-objective optimization of mechanical and thermal characteristics of a

- bipolar plate for use in a proton exchange membrane fuel cell Energy Rep 8:2747–2761. <https://doi.org/10.1016/j.egy.2022.01.199>
- Bernardi DM (1990) Water-balance calculations for solid-polymer-electrolyte fuel cells. *J Electrochem Soc* 137:3344–3350. <https://doi.org/10.1149/1.2086220>
- Bernardi DM, Verbrugge MW (1992) A mathematical model of the solid-polymer-electrolyte fuel cell. *J Electrochem Soc* 139:2477–2491. <https://doi.org/10.1149/1.2221251>
- Berning T (2002) Phenomena in a PEM fuel cell
- Freire L, Antolini E, Linardi M, Santiago E, Passos R (2014) Influence of operational parameters on the performance of PEMFCs with serpentine flow field channels having different (rectangular and trapezoidal) cross-section shape. *Int J Hydrogen Energy* 39:12052–12060. <https://doi.org/10.1016/j.ijhydene.2014.06.041>
- Fuller TF, Newman J (1993) Water and thermal management in solid-polymer-electrolyte fuel cells. *J Electrochem Soc* 140:1218–1225. <https://doi.org/10.1149/1.2220960>
- Görgün H, Arcak M, Barbir F (2006) An algorithm for estimation of membrane water content in PEM fuel cells. *J Power Sources* 157:389–394. <https://doi.org/10.1016/j.jpowsour.2005.07.053>
- Gurau V, Liu H, Kakaç S (1998) Two-dimensional model for proton exchange membrane fuel cells. *AIChE J* 44:2410–2422. <https://doi.org/10.1002/aic.690441109>
- Henriques T, César B, Branco P (2010) Increasing the efficiency of a portable PEM fuel cell by altering the cathode channel geometry: a numerical and experimental study. *Appl Energy* 87:1400–1409. <https://doi.org/10.1016/j.apenergy.2009.09.001>
- Hu M, Gu A, Wang M, Zhu X, Yu L (2004) Three dimensional, two phase flow mathematical model for PEM fuel cell: part I. Model development. *Energy Convers Manag* 45:1861–1882. <https://doi.org/10.1016/j.enconman.2003.09.022>
- Jia Y, Zeng M, Barnoon P, Toghraie D (2021) CFD simulation of time-dependent oxygen production in a manifold electrolyzer using a two-phase model. *Int Commun Heat Mass Transf* 126:105446. <https://doi.org/10.1016/j.icheatmasstransfer.2021.105446>
- Kanchan BK, Randive P, Pati S (2020) Numerical investigation of multi-layered porosity in the gas diffusion layer on the performance of a PEM fuel cell. *Int J Hydrogen Energy* 45:21836–21847. <https://doi.org/10.1016/j.ijhydene.2020.05.218>
- Kone J-P, Zhang X, Yan Y, Hu G, Ahmadi G (2018) CFD modeling and simulation of PEM fuel cell using OpenFOAM. *Energy Proc.* 145:64–69. <https://doi.org/10.1016/j.egypro.2018.04.011>
- Kyriakopoulos GL, Aravossis KG (2023) Literature review of hydrogen energy systems and renewable energy sources. *Energies* 16. <https://doi.org/10.3390/en16227493>
- Kyriakopoulos GL, Sebos Iv Enhancing climate neutrality and resilience through coordinated climate action: review of the synergies between mitigation and adaptation actions. *Climate* 11. <https://doi.org/10.3390/cli11050105>
- Lee D, Bae J (2012) Visualization of flooding in a single cell and stacks by using a newly-designed transparent PEMFC. *Int J Hydrogen Energy* 37:422–435. <https://doi.org/10.1016/j.ijhydene.2011.09.073>
- Mei B, Barnoon P, Toghraie D, Su C-H, Nguyen HC, Khan A (2022) Energy, exergy, environmental and economic analyzes (4E) and multi-objective optimization of a PEM fuel cell equipped with coolant channels. *Renew Sustain Energy Rev* 157:112021. <https://doi.org/10.1016/j.rser.2021.112021>
- Kermani MJ, Ghanbarian A (2014) Performance improvement of PEM fuel cells using air channel indentation; part i: mechanisms to enrich oxygen concentration in catalyst layer. *Iran J Hydrog Fuel Cell* 1:199–207. http://ijhfc.irost.ir/article_96.html
- Nguyen TV, White RE (1993) A water and heat management model for proton-exchange-membrane fuel cells. *J Electrochem Soc* 140:2178–2186. <https://doi.org/10.1149/1.2220792>
- Nguyen PT, Berning T, Djilali N (2004) Computational model of a PEM fuel cell with serpentine gas flow channels. *J Power Sources* 130:149–157. <https://doi.org/10.1016/j.jpowsour.2003.12.027>
- Rostami L, Mohamad Gholy Nejad P, Vatani A (2016) A numerical investigation of serpentine flow channel with different bend sizes in polymer electrolyte membrane fuel cells. *Energy*. 97:400–410. <https://doi.org/10.1016/j.energy.2015.10.132>
- Scholta J, Escher G, Zhang W, Küppers L, Jörissen L, Lehnert W (2006) Investigation on the influence of channel geometries on PEMFC performance. *J Power Sources* 155:66–71. <https://doi.org/10.1016/j.jpowsour.2005.05.099>
- Sivertsen BR, Djilali N (2005) CFD-based modelling of proton exchange membrane fuel cells. *J Power Sources* 141:65–78. <https://doi.org/10.1016/j.jpowsour.2004.08.054>
- Sun L, Oosthuizen PH, McAuley KB (2006) A numerical study of channel-to-channel flow cross-over through the gas diffusion layer in a PEM-fuel-cell flow system using a serpentine channel with a trapezoidal cross-sectional shape ☆☆A preliminary version of this paper was presented at ICMM05: third. *Int J Therm Sci* 45:1021–1026. <https://doi.org/10.1016/j.ijthermalsci.2006.01.005>
- Tamerabet M, Moussa H, Youcef S, Abdallah M (2017) Unsteady three-dimensional numerical study of mass transfer in PEM fuel cell with spiral flow field. *Int J Hydrogen Energy* 42. <https://doi.org/10.1016/j.ijhydene.2016.12.084>
- Vazifeshenas Y, Sedighi K, Shakeri M (2015) Numerical investigation of a novel compound flow-field for PEMFC performance improvement. *Int J Hydrogen Energy* 40. <https://doi.org/10.1016/j.ijhydene.2015.08.077>
- Wang L, Husar A, Zhou T, Liu H (2003) A parametric study of PEM fuel cell performances. *Int J Hydrogen Energy* 28:1263–1272. [https://doi.org/10.1016/S0360-3199\(02\)00284-7](https://doi.org/10.1016/S0360-3199(02)00284-7)
- Wang X-D, Lu G, Duan Y-Y, Lee D-J (2012) Numerical analysis on performances of polymer electrolyte membrane fuel cells with various cathode flow channel geometries. *Int J Hydrogen Energy* 37:15778–15786. <https://doi.org/10.1016/j.ijhydene.2012.04.028>
- Yi JS, Van Nguyen T (1998) An along-the-channel model for proton exchange membrane fuel cells. *J Electrochem Soc* 145:1149–1159
- You L, Liu H (2002) A two-phase flow and transport model for the cathode of PEM fuel cells. *Int J Heat Mass Transf* 45:2277–2287. [https://doi.org/10.1016/S0017-9310\(01\)00322-2](https://doi.org/10.1016/S0017-9310(01)00322-2)
- Zhang Y, Li X, Klinkova A (2021) Numerical investigation of delamination onset and propagation in catalyst layers of PEM fuel cells under hygrothermal cycles. *Int J Hydrogen Energy* 46:11071–11083. <https://doi.org/10.1016/j.ijhydene.2020.09.258>

Publisher's Note Springer Nature remains neutral with regard to jurisdictional claims in published maps and institutional affiliations.

Springer Nature or its licensor (e.g. a society or other partner) holds exclusive rights to this article under a publishing agreement with the author(s) or other rightsholder(s); author self-archiving of the accepted manuscript version of this article is solely governed by the terms of such publishing agreement and applicable law.